PAPER

Check for updates

Carbazole–acenaphthene (donor–acceptor)-based luminophores for picric acid detection: a combined experimental and theoretical study†

Aravind Babu Kajjam, Kasturi Singh, [ID] R. V. Varun Tej and Sivakumar Vaidyanathan [ID] *

In the present investigation, carbazole–acenaphthene-based donor–acceptor luminophores were designed and synthesized. All the luminophores showed fluorescence quenching behavior towards nitroaromatics through complex formation. All the luminophores were used for the detection of picric acid (PA) based on fluorescence quenching. All the luminophores showed the highest quenching efficiency with PA, compared with that of other explosives like 2,4-dinitrophenol (2,4-DNP), 4-nitrophenol (NP), benzoic acid (BA), and phenol (PH). Fluorescence quenching behavior was confirmed by ^{1}H NMR, fluorescence and DFT studies. The time-resolved fluorescence results indicate that the dynamic quenching mechanism is involved in PA detection. The photo-induced electron transfer (PET) from luminophores to PA was confirmed by NMR and DFT analyses. DFT calculations of luminophores with PA were also carried out to know the energy levels of the complex formed after the addition of PA. In addition, the detection limit, *i.e.*, the photographic detection of PA, has been successfully demonstrated in the solution and solid states (TLC plates). The singlet and triplet energy states of the excited molecules were calculated through time-dependent density functional theory (TD-DFT) calculations.

Introduction

Efficient designs of luminophores have drawn significant interest in the identification of explosives in the field of environmental pollution control and better combat terrorism.[1,2] This is an important challenge for national security, environmental protection and bio-analysis applications in recent decades.[3] The principal constituents of many explosives are various nitroaromatic compounds such as trinitrotoluene (TNT), 2,4-dinitrophenol (2,4-DNP) and picric acid (PA). Detection of picric acid (PA) compared to other nitroaromatic compounds is very essential, as the explosive nature of PA has been used to prepare weapons such as bombs and grenades. In addition, PA can cause damage to the skin, aggravation of the eyes, sickliness, cancer, lung damage and damage to respiratory organs.[4] In the last two decades, a variety of strategies have been used to distinguish PA, for example, gas chromatography, mass

spectrometry (GC-MS), particle versatility spectrometry (IMS), electrochemical techniques, surface-improved Raman spectroscopy, *etc.*,[5] Generally, electron-deficient nitroaromatics are anticipated to quench fluorescence through photo-induced electron transfer processes for electron-rich compounds, which constitute a strong basis for their applications in the detection of explosives. However, these exorbitant instrumental systems are difficult to manage and have restrictions for their practical applications. Alternatively, simple procedures were used to distinguish nitroaromatics that allow a few points of interest such as low cost, rapid reaction and high selectivity.[6] In contrast to all simple techniques, fluorescence quenching is one of the most effective methods to detect nitroaromatic explosives.[7–10]

To date, many scientists have been studying fluorescent organic molecules for the detection of nitroaromatics, including small molecular dyes, conjugated polymers, fluorescent metal-natural systems, metal organic frameworks (MOFs), quantum dots, gold nanoparticles, and fluorescent molecular assemblies.[11,12,28] Most of the reports available to identify nitroaromatics, however, lack high selectivity, resulting in poor PA signal amplification. To date, significant efforts have been made to synthesize new and efficient organic luminophores (luminescent materials) that can detect PA (and nitroaromatics). Although, searching for new luminescent materials

Department of Chemistry, National Institute of Technology, Rourkela 769008, Odisha, India. E-mail: vsiva@nitrkl.ac.in; Tel: +91-661-2462654
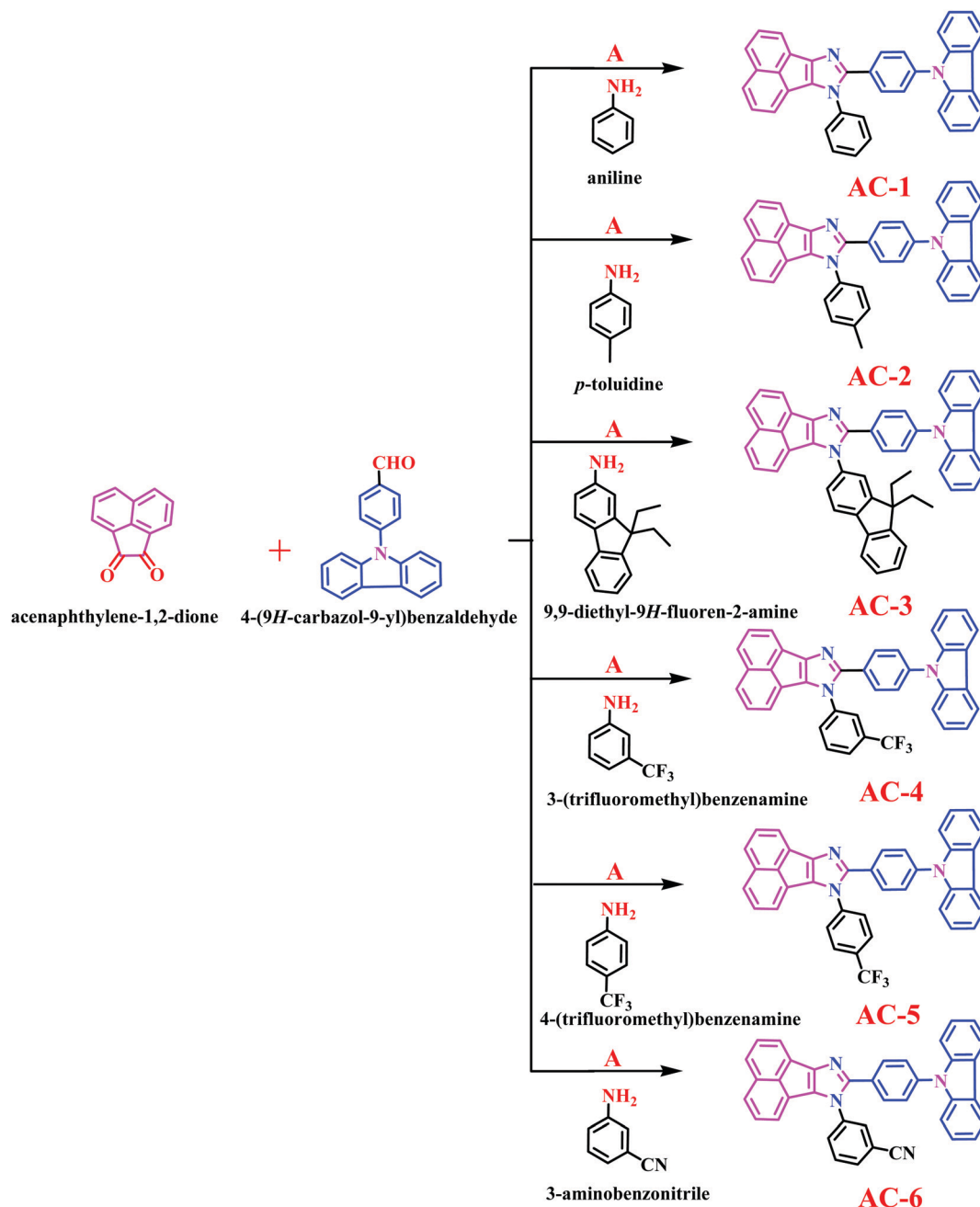
† Electronic supplementary information (ESI) available: Synthesis, copies of NMR spectra, copies of mass spectra, and chemosensor data including photoluminescence spectra, lifetime measurements, cyclic voltammetry analysis, tables of single crystal data, and tables and images of DFT analysis. CCDC 1568852 (**AC-1**), 1568853 (**AC-2**) and 1571347 (**AC-5-PA**). For ESI and crystallographic data in CIF or other electronic format see DOI: 10.1039/d1ma00445j

with optical response (*e.g.* color changes or varying fluorescence) is still highly desirable because this type of detection has a fast response, high sensitivity, low cost, and simple sample preparation. It is well known that imidazole derivatives are considered to be excellent luminogens and have been demonstrated to show excellent optical responses in the field of OLEDs (including ligand for Eu-complexes),[13] biomedicine,[14] supramolecular chemistry,[15] coordination chemistry[16] and CO_2 chemosensors.[17] However, very few examples of imidazole-based materials were used as sensors for the detection of nitroaromatics.[18] In addition, acenaphthene derivatives have a variety of biological properties[19] and are widely used in

pharmaceutical applications,[20] despite the fascinating spectrum of biological activities and luminogen properties in the acenaphthene group and imidazole linkages, integration of both the moieties in one chromophore and their effects on photophysical properties. In addition, to the best of our knowledge, there is no report on acenaphthene-based luminophores for PA sensing.

Herein, we report a series of new conjugated imidazole derivatives, acenaphtho[1,2-*d*]imidazole (electron-deficient center) moiety and carbazole (electron-rich center) moiety, as efficient sensor materials for the selective detection of trace amounts of picric acid at ppb levels. As shown in Scheme 1, six

Scheme 1 The synthetic procedure of the designed luminophores.

new luminophores were successfully prepared, namely, 8-(4-(9H-carbazol-9-yl)phenyl)-7-phenyl-7H-acenaphtho[1,2-d]imidazole (AC-1), 8-(4-(9H-carbazol-9-yl)phenyl)-7-p-tolyl-7H-acenaphtho[1,2-d]imidazole (AC-2), 8-(4-(9H-carbazol-9-yl)phenyl)-7-(9,9-diethyl-9H-fluoren-2-yl)-7H-acenaphtho[1,2-d]imidazole (AC-3), 8-(4-(9H-carbazol-9-yl)phenyl)-7-(3-(trifluoromethyl)phenyl)-7H-acenaphtho[1,2-d]imidazole (AC-4), 8-(4-(9H-carbazol-9-yl)phenyl)-7-(4-(trifluoromethyl)phenyl)-7H-acenaphtho[1,2-d]imidazole (AC-5), and 3-(8-(4-(9H-carbazol-9-yl)phenyl)-7H-acenaphtho[1,2-d]imidazol-7-yl)benzonitrile (AC-6). Herein, we present a detailed account of their photophysical, electrochemical, and theoretical analyses. Fluorescence quenching was performed on various explosives such as benzoic acid (BA), phenol (PH), 4-nitrophenol (4-NP), 2,4-dinitrophenol (2,4-DNP) and picric acid (PA). Photophysical, electrochemical and PA detection mechanisms have been verified by density functional theory calculations. A single-step method shown in Scheme S1 (ESI†) was used to obtain the acenaphthene-imidazo derivatives connected by different conjugation units such as benzene, toluidine, fluorene, 4-(trifluoromethyl)phenyl, 3-(trifluoromethyl)phenyl and benzonitrile at the N1 position. All the luminophores have donor–acceptor (D–A) structures, which contain the elementary units of electron-donating carbazole and electron-accepting acenaphthene-imidazole group. The only difference in the luminophores was the different conjugation units at the N1 position. The reaction of the corresponding aldehyde to the ketone in the presence of ammonium acetate produced the desired target luminophores in good yields (ESI†). The molecular compositions of the yellowish-orange luminophores were unambiguously established by ^{1}H, ^{13}C NMR, and high-resolution mass spectrometry measurements and some of them were crystallographically characterized. Finally, these acenaphthene-imidazo luminophores were used for detecting

nitroaromatics. Fortunately, these luminophores (with good selectivity and high sensitivity) can be used for PA detection in both solution and contact modes (TLC plates) (Fig. 1).

Results and discussion

Single crystal analysis of AC-1 and AC-2 luminophores was carried out to understand their structural properties such as bond angles and bond lengths. Fig. 2 shows the ORTEP diagrams of AC-1 and AC-2 luminophores, and the corresponding refinement parameters, bond lengths and bond angles, are tabulated in Tables ST1–ST5 (ESI†). An attempt has been made to crystallize the other luminophores (AC-3 to AC-6); however, the attempts failed.

All the luminophores exhibited nearly identical absorption (Fig. 3a and Table 1) and emission behaviors (Fig. 3b), except for a slight red-shifting tendency in the luminophores as a result of the introduction of different conjugated groups at the N1 position. In Fig. 3a, the absorption spectra of luminophores display four well-defined absorption peaks. The strong absorption peaks at ~290, ~325, and ~340 nm can be assigned to π–π* transitions and the other weak absorption peaks around 400–450 nm can be assigned to n–π* transitions.[21,22] The UV-Vis absorption titrations were performed to get a quantitative idea of the interaction of PA with the luminophores at room temperature (Fig. S24–S29, ESI†). While increasing the PA concentration to that of the luminophores, a slight increase in the absorption peaks was observed, indicating the formation of a ground-state complex between the luminophores and PA *via* charge transfer transitions.[23] When dilute solutions of
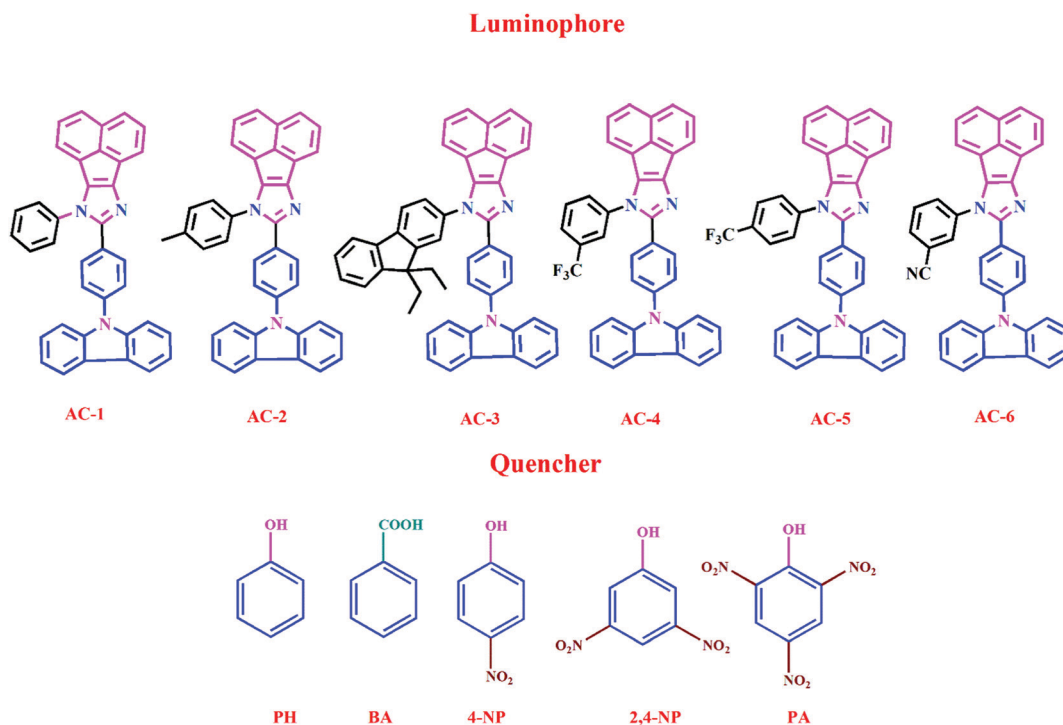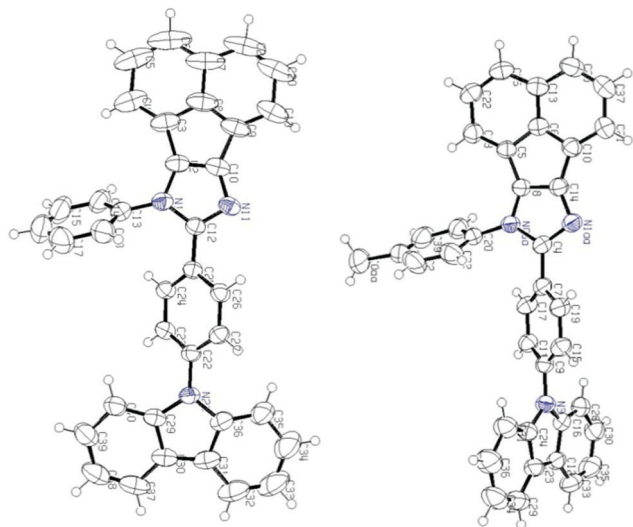
Luminophore

Quencher

Fig. 1 Chemical structures of acenaphthene-imidazo-based luminophore (top) quenchers used for chemosensors (bottom).

Fig. 2 ORTEP diagrams of AC-1 and AC-2 luminophores (50% probability ellipsoids; H atoms and co-crystallized solvent molecules are omitted). N atoms in blue color (CCDC 1568852 (AC-1) and CCDC 1568853 (AC-2)†).

Table 1 Photophysical and CIE chromaticity values of all luminophores (AC-1 to AC-6)

Luminophores	$\lambda_{abs}{}^a$ (nm)	λ_{em} (nm)	PLQY (Φ) (%)	Lifetime (μs)	CIE coordinates (x, y)
AC-1	293, 325, 339, 411	556	15.2	1.12	0.37, 0.46
AC-2	291, 326, 340, 410	558	11.6	2.37	0.42, 0.52
AC-3	309, 422	547	10.5	1.72	0.36, 0.48
AC-4	274, 335, 351, 394	564	14.3	1.24	0.43, 0.51
AC-5	281, 325, 339, 415	566	16.5	2.15	0.46, 0.51
AC-6	280, 325, 340, 416	571	19.1	1.36	0.45, 0.52

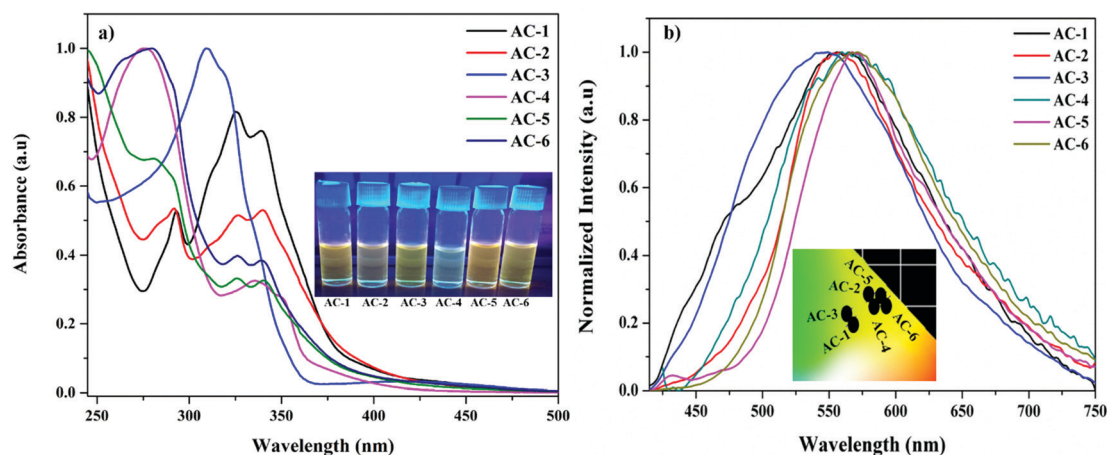^{a} In dichloromethane (CH_2Cl_2) solution (1×10^{-5} M).

Table 2 Electrochemical analysis of luminophores

Ligand	E_{ox} (V)	E_{red} (V)	HOMO (eV)	LUMO (eV)	Band gap (eV)
AC-1	1.107	−1.329	−5.507	−3.071	2.436
AC-2	1.301	−1.108	−5.701	−3.292	2.409
AC-3	1.399	−1.540	−5.799	−2.860	2.939
AC-4	1.138	−1.168	−5.538	−3.232	2.306
AC-5	1.127	−1.107	−5.527	−3.293	2.234
AC-6	1.107	−1.077	−5.507	−3.323	2.184

E_{red}^{onset} = the onset reduction potentials; E_{oxd}^{onset} = the onset oxidation potentials; $E_{LUMO} = -e(E_{red}^{onset} + 4.4)$; E_g = band gap = $E_{HOMO} - E_{LUMO}$.

luminophores are treated with PA, the solutions immediately changed from yellow to colorless under UV light.

The fluorescence spectra of the luminophores show intense yellowish emission at 547–571 nm (Fig. 3b) with the corresponding excitation wavelength (Table 2). The sensing behavior of all the luminophores was studied in THF (1×10^{-6} M) with different nitro-containing compounds such as phenol (PH), benzoic acid (BA), 2,4-dinitrophenol (2,4-DNP), 4-nitrophenol (4-NP), and picric acid (PA) (Fig. S30–S34, ESI†). The fluorescence spectral changes were observed upon the addition of PA. Fig. 4a shows the decreasing intensity of the luminophores with an increasing PA concentration.

To evaluate the quenching efficiency of the luminophores, fluorometric analysis of the luminophores was performed to transform the PA data to Stern–Volmer plots.[22] The quenching constant was calculated by using the Stern–Volmer equation:[22]

$$I_0/I = 1 + K_{SV}[Q]$$

where I_0 and I are the PL intensities before and after the addition of PA, [Q] is the quencher concentration and K_{SV} is the Stern–Volmer or quenching constant (Fig. 4b).

The fluorescence and the Stern–Volmer plots (I_0/I vs. PA concentration) of all the luminophores (AC-1 to AC-6) are presented in Fig. 4 and Fig. S35–S39 (ESI†). The Stern–Volmer constant of all the luminophores was found to be in the range from 9.16×10^4 to 2.43×10^5 M^{-1} (Table ST6, ESI†), which is comparable to the reported values.[24] It has been shown that the Stern–Volmer plots (Fig. 4b) gave curves bending upward (due to the super amplified quenching effect),[25] suggesting that

Fig. 3 (a) UV-Vis absorption spectra (inset images under UV light) and (b) emission spectra (inset: CIE plot) of the synthesized luminophores.
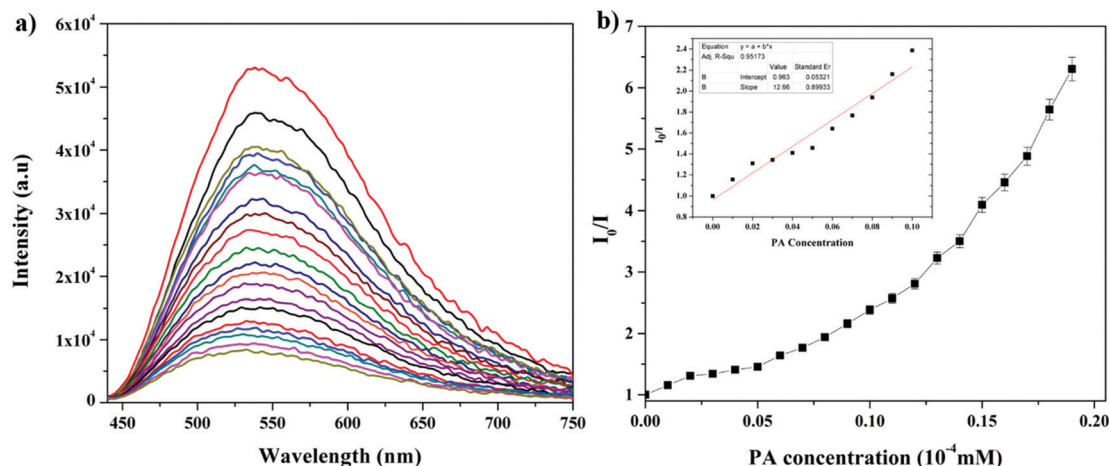
Fig. 4 (a) Change in the fluorescence of AC-1 upon the addition of PA. (b) Stern–Volmer plots of AC-1 using PA as a quencher. Inset: Stern–Volmer plots at lower concentration region of PA.

when the PA concentration increased, the emission (luminescence) quenching becomes more efficient. The linear Stern–Volmer curve was observed when the PA concentration was relatively low (inset in Fig. 4b). The remaining luminophores' (AC-2 to AC-6) fluorescence spectra with PA and Stern–Volmer plots are presented in the ESI.† Compared to all the luminophores, the quenching constant of AC-2 and AC-6 was higher than those of some PA-reported sensors (refer Table ST6 in the ESI†). This may be related to the highest LUMO (-1.769 eV, Table 3) level of the AC-2, and the electrons are easily transferred from AC-2 to PA. Similarly, the K_{SV} values of AC-1, AC-3, AC-4 and AC-5 were also calculated to be 1.26×10^5, 1.2×10^5, 9.16×10^4 and 1.14×10^5 M^{-1}, respectively (Table ST6 in the ESI†). To determine the quenching mechanism of the luminophores, it is necessary to measure the lifetime of the luminophores. The lifetime measurement data of all the luminophores (AC-1 to AC-6) are summarized in the ESI† (Fig. S39 and Table ST7). In all the cases, the decay of the luminophores in chloroform solution was bi-exponentially fitted, and the average lifetime of the luminophores was in the range of 2.59–6.64 ns. However, after the addition of the quencher (PA) to luminophores, a reduction in the lifetime was observed (Fig. S40–S42 and Table ST7, ESI†). This shows the dynamic quenching by transferring electrons from the luminophores to the quencher molecule after the addition of PA.[24a] In addition, the digital photograph (Fig. 10) clearly shows that the fluorescence color has changed from orange to colorless. Interestingly, the quenching efficiency of all the luminophores toward picric acid was found in the range of 83–95%, which indicates the effectiveness to detect PA over other nitroaromatics. Fig. 5a clearly shows that the PA quenching efficiency of AC-6 and AC-2 was higher compared to that of the other luminophores. The quenching behavior of AC-6 with different explosives is shown in Fig. 5b. Similarly, the quenching efficiencies of AC-1, AC-2, AC-3, AC-4 and AC-5 were also calculated to be, 84, 90, 84, 88 and 83%, respectively (Fig. 5a). The quenching phenomena and their luminescence efficiency plots of the remaining luminophores (AC-1 to AC-5) with other explosives are displayed in the ESI† (Fig. S43–S46). It is clearly indicated that the sensitivity of these luminophores to PA is high compared to that of all other explosives.

The PA detection limit can be obtained by measuring the fluorescence of the luminophores (AC-1 to AC-6, 10^{-4} M) in THF with PA solution (10^{-6} M). The corresponding fluorescence intensity as a function of added PA is plotted and shown in Fig. 6. The PA detection limit (DL) can be calculated by using the following equation:[24b]

$$DL = C_L \times C_T \qquad (1)$$

Table 3 Theoretical data of all luminophores (AC-1 to AC-6) and luminophores with PA

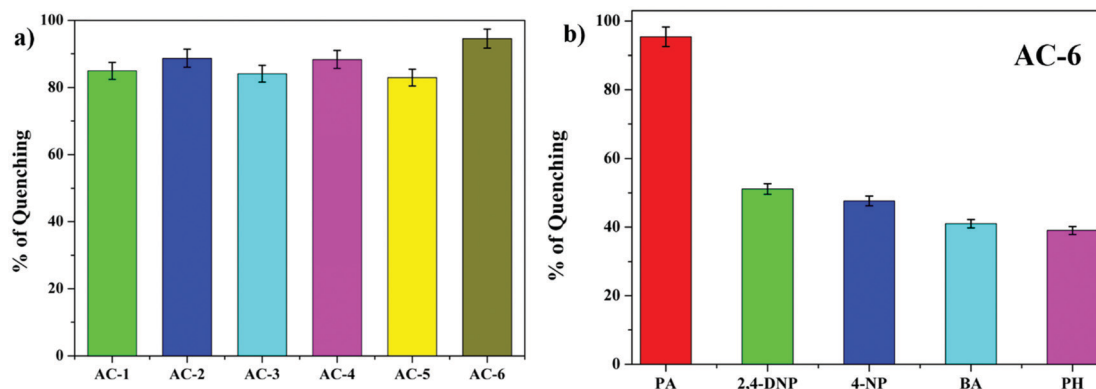| Compound	HOMO (eV)	LUMO (eV)	HOMO−1 (eV)	LUMO+1 (eV)	Band gap (eV)	Singlet (eV)	Triplet (eV)
AC-1	−5.071	−1.801	−5.489	−1.036	3.270	2.6687	2.0658
AC-1 + PA	−5.466	−2.594	−5.800	−2.412	2.872	—	—
AC-2	−5.042	−1.768	−5.469	−0.998	3.274	2.6654	2.0659
AC-2 + PA	−5.297	−3.006	−5.712	−2.706	2.291	—	—
AC-3	−5.043	−1.769	−5.472	−1.269	3.274	2.6668	2.0698
AC-3 + PA	−5.422	−2.515	−5.756	−2.379	2.07	—	—
AC-4	−5.200	−1.934	−5.594	−1.302	3.266	2.6882	2.0651
AC-4 + PA	−5.379	−3.197	−5.778	−2.882	2.182	—	—
AC-5	−5.198	−1.970	−5.600	−1.365	3.227	2.675	2.0662
AC-5 + PA	−5.361	−3.201	−5.754	−2.884	2.160	—	—
AC-6	−5.217	−2.041	−5.613	−1.904	3.175	2.6532	2.0531
AC-6 + PA	−5.417	−3.285	−5.811	−2.957	2.132	—	—

Fig. 5 (a) Fluorescence quenching efficiencies of all luminophores in PA. (b) Fluorescence quenching efficiencies of AC-6 towards different analytes.

where C_L is the concentration of luminophores, and C_T is the concentration of PA at which a steep decrease is observed. The detection limits of the currently synthesized luminophores are in the range of 50–450 ppb (Table ST6, ESI†), which show better sensitivity than most of the small molecular fluorescent PA sensors previously reported (for more examples, see Table ST23 in the ESI†).[25] Compared to all the luminophores, AC-2 has the highest sensitivity towards PA indeed. This may be because AC-2 with methyl as an electron-donating group more easily interacts with the electron-deficient PA than the others.[25c]

Fig. 7 demonstrates the feasible PA detection mechanism owing to the strong acid behavior of PA. It can easily transfer the acidic protons to the basic functional group in the lumino-phores. Because of the presence of the basic N atom on the imidazole ring of the luminophores, it can strongly interact with the acidic PA, leading to fluorescence quenching. The ^{1}H NMR technique was also used to clarify the interaction between the luminophores and the PA. As shown in Fig. 7, the shift of the PA proton signal in the NMR spectra confirms the formation of a complex with acenaphthene-imidazo nitrogen and PA. The proton signal of the AC-2 luminophore was moved up-field from 8.16 ppm to 8.12 ppm after the addition of excess PA, supporting the strong electrostatic interaction between the PA and the AC-2 luminophore. The results showed that the PET process could play a major role in the fluorescence sensing of the AC-2 luminophore towards PA. The ^{1}H NMR spectra of the remaining acenaphthene-imidazo derivatives with PA are shown in the ESI† (Fig. S48–S51).

Fortunately, a good-quality AC-5-PA single crystal was grown using the slow vapor diffusion method (a dichloromethane solution of AC-5 and PA was used) and later, an X-ray diffraction study was performed for the hybrid crystal. The ORTEP diagram of AC-5 with picric acid is shown in Fig. 8. The figure and crystal data clearly indicate the complex formation by the transfer of picric acid protons to the imidazole group. Table ST11 (ESI†) clearly shows that there is a strong N–H–O interaction between the imidazole moiety (N2) and the oxygen atom (O46) picrate ion. The detailed bond lengths, bond angles and hydrogen
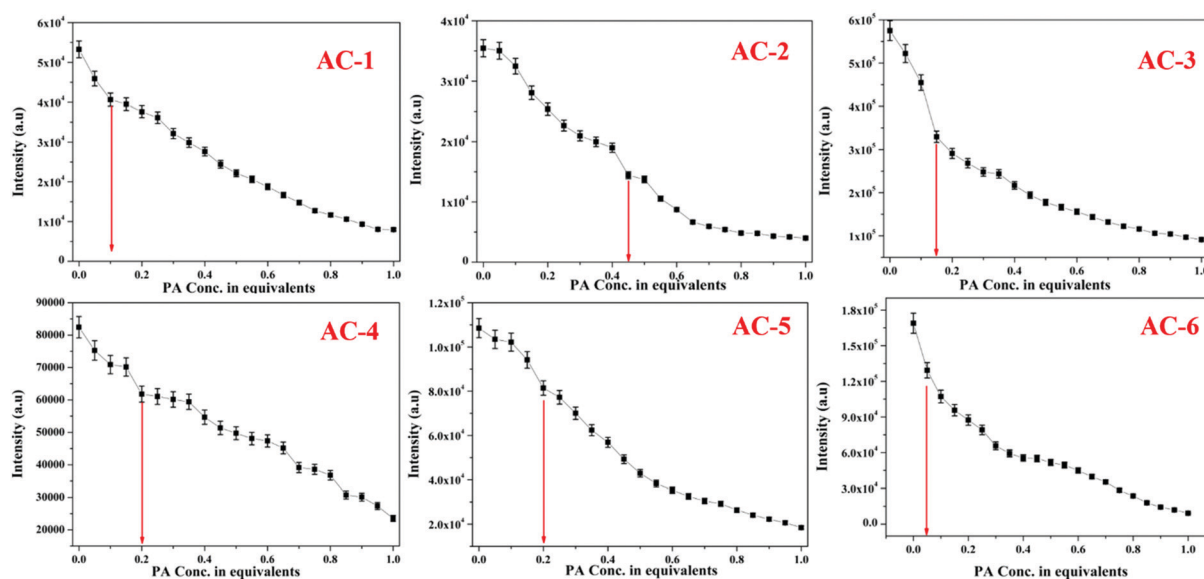

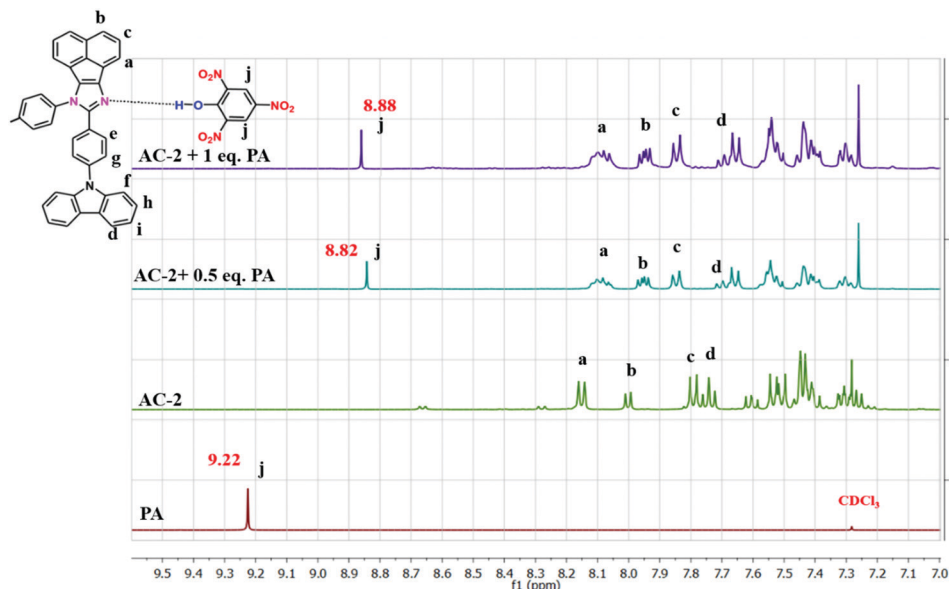**Fig. 6** Fluorescence intensity of luminophores as a function of PA concentration.

Fig. 7 ^{1}H-NMR spectra of AC-2 with PA in CDCl$_3$.

bonds of AC-5-PA are tabulated in Tables ST8–ST11 (ESI†) (Fig. 9).

Although the single crystal of AC-6-PA was obtained (Fig. 10), the quality of diffraction and fitting is comparatively not good. The detailed crystal information of AC-6-PA is given in the ESI† (Fig. S53 and Table ST12–ST14, ESI†).

It is well known that during the preparation and packaging of explosive devices, partial explosive contamination on clothing, human body, and other materials in the ambience has been observed.[26] In such cases, the contamination of the explosive chemicals can be easily checked in the contact mode. To ensure this, TLC plates are prepared by spotting a THF solution of luminophores on TLC. All the luminophores show orange emission in the TLC plates and become non-emissive when the PA solution is absorbed by the luminophores (Fig. 10, bottom). The

fluorescence quenching phenomenon is observed by the addition of PA solution under UV light (Fig. 10, top).

Electrochemical analysis

The electrochemical properties of the luminophores were studied by cyclic voltammetry (CV). All the luminophores were electrochemically stable and there was one reversible or quasi-reversible redox peak observed for each molecule under CV conditions (Fig. 11). The reversible one-electron oxidation process around 1.10–1.39 eV was derived from the acenaphthene-imidazole moiety. These obtained results suggest that all the compounds possess good hole and electron transport properties. There is little difference in the LUMO of all the compounds, which would be attributed to the conjugation and substitution of the group, whereas the HOMO energy levels are located in the same range and there is no difference among them. Compared with all the materials, AC-6 has shown a low band gap due to the presence of the electron-withdrawing cyanide (CN) group at the *meta*-position of the benzene ring and is correlated with the photoluminescence data. The detailed electrochemical data of the synthesized luminophores are tabulated in Table 2.

DFT analysis

Frontier molecular orbital properties. The optimized structures of all the luminophores (AC-1 to AC-6) are shown in Fig. 12. To understand the photophysical properties of these luminophores, the frontier molecular orbital energies as well as the HOMO and LUMO contour plots of the investigated materials are plotted in Fig. 13 and Fig. ST15 (ESI†). Table 3 reveals the calculated HOMO–LUMO levels and their energy levels (singlet and triplet). Table ST15 (ESI†) shows small differences in the electron density distribution (population) of the HOMOs of all the compounds which are all mainly localized on the
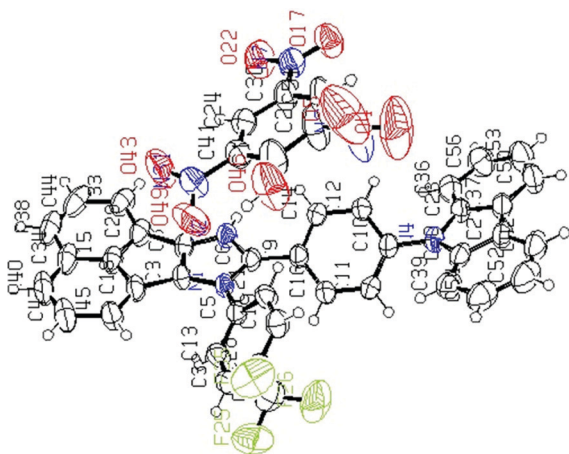

Fig. 8 ORTEP diagrams of AC-5 with picric acid (50% probability ellipsoids; H atoms and co-crystallized solvent molecules are omitted). N atoms in blue, F atoms in green and O atoms in red (CCDC 1571347†).
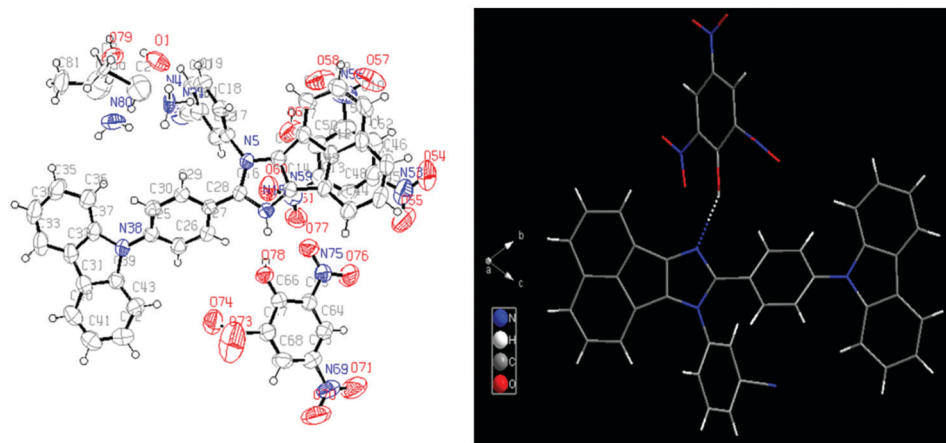
Fig. 9 ORTEP diagram of AC-6 with picric acid (left). Wire and stick structures of AC-6 with picric acid using Diamond software (solvent molecules are omitted) (right). N atoms in blue, C atoms in gray and O atoms in red.
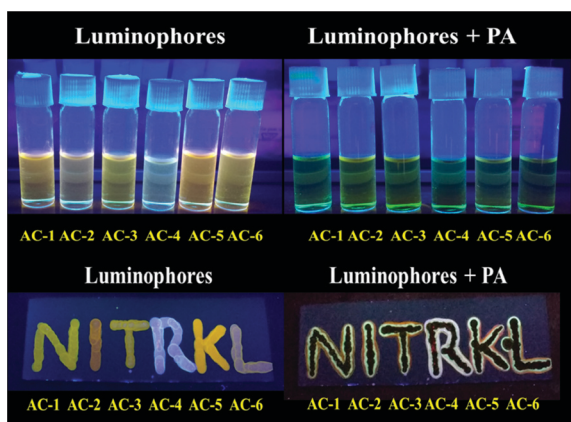

Fig. 10 Images of solution (top) with luminophores under UV light before and after adding PA. Images of TLC plates (bottom) observed with the luminophores under UV light before and after adding PA.

carbazole and little on the acenaphthene group. However, unlike in the case of HOMOs, the six studied materials have shown a great difference in the electron density distribution of the LUMOs. For AC-1 to AC-3, the LUMO is primarily contributed from the acenaphthene group of the molecule as well as a little contribution from the imidazole moiety. Compared with AC-1 to AC-3, the absence of heteroatoms in these molecules does not have a great influence on the electron density distribution of the LUMO. In contrast, the introduction of CF_3 and CN groups has a great influence on the electron density distribution of the LUMO. Additionally, different substitution positions of the CF_3 group also show little difference in the LUMO electron density distribution. For example, when the CF_3 moiety is attached at the *para*-position of the phenyl ring of the molecule, the LUMO is localized more on the phenyl ring of the molecule when compared to its *meta*-substituted analogue. Here, it should be noted that the electron density distribution of the LUMOs for the luminophores with the CF_3 group is quite different from that without the CF_3 group, whereas the electron density distribution of the LUMOs for the molecules with the CF_3 group is more similar to that with the CN group, suggesting that the CF_3 and CN groups have a great influence on the electron density distribution of the LUMOs. The different types of molecular orbitals will absolutely influence the electronic
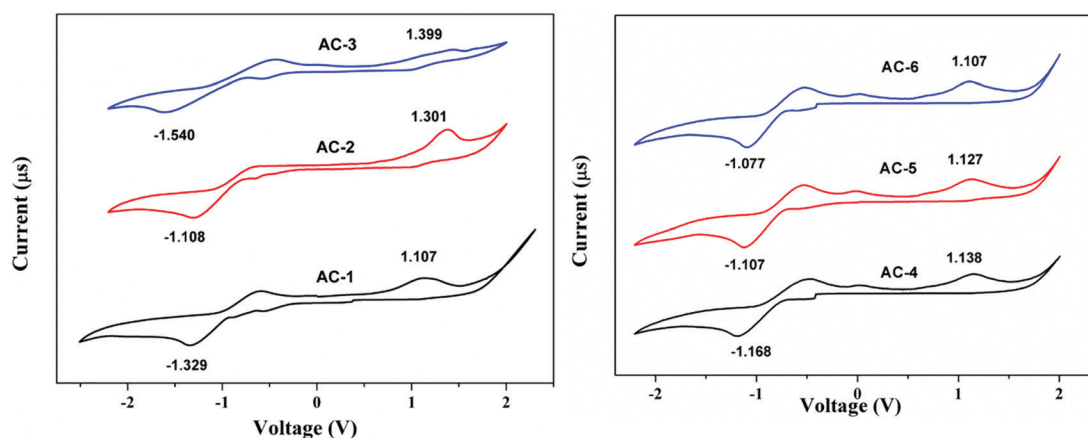

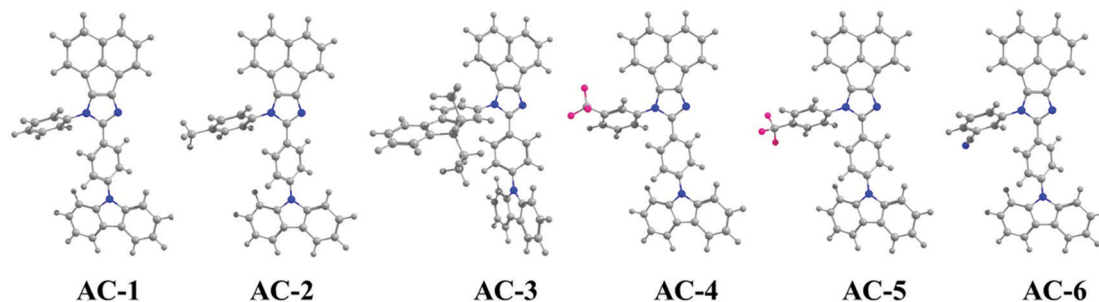**Fig. 11** Cyclic voltammetry diagram of acenaphthene-based luminophores.

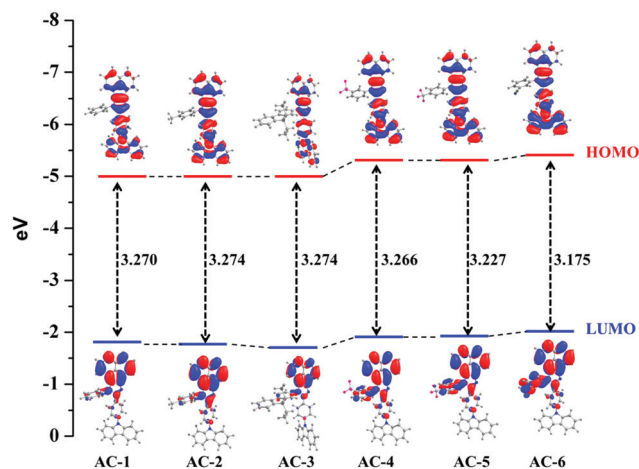**Fig. 12** Optimized structures of acenaphthene-based luminophores.

Fig. 13 Energy-level diagram of the luminophores (AC-1 to AC-6).
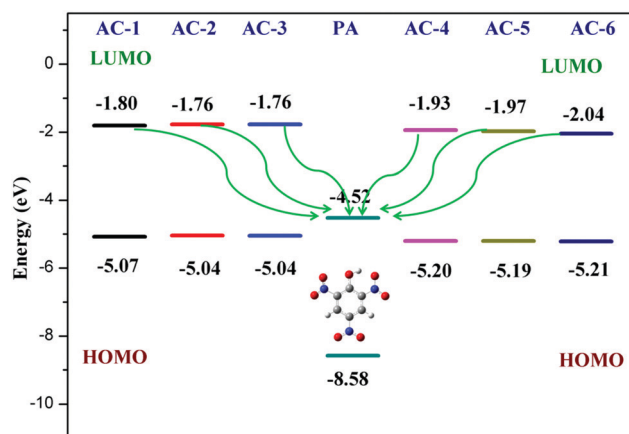

Fig. 14 Electron transfer process between the luminophores (AC-1 to AC-6) and PA.

transition character upon excitation, which will be further explained in detail in the electronic absorption spectra. The detailed theoretical absorption spectra and their corresponding singlet energy levels of all the luminophores are explained in the ESI† (Fig. S59 and Table ST16).

Furthermore, the calculated LUMO energy level of the PA (E_{LUMO} = −4.52 eV) is between the calculated LUMO (E_{LUMO} = −1.08 eV) and HOMO (E_{HOMO} = −4.99 eV) energy levels of all the luminophores (AC-1 to AC-6) Fig. 14 shows that the photo-induced electron transfer (PET) process is the main possible contribution to the fluorescence quenching of the luminophores by the addition of PA.

To understand the origin of PA sensitivity, the frontier molecular orbitals of PA and AC derivatives (AC-1 to AC-6) were determined by density functional theory (DFT) computational studies based on the B3LYP/6-31G basis set. Furthermore, the calculated LUMO energy level of the PA (E_{LUMO} = −4.58 eV) is between the calculated LUMO (E_{LUMO} = −1.76 to −2.04 eV) and HOMO (E_{HOMO} = −5.04 to −5.21 eV) energy levels of the AC luminophores (Fig. 14 and 15), suggesting that the photo-induced electron transfer (PET) process is the possible main contribution to the fluorescence quenching.[26] The significant reduction in the electron density on the N atom upon the binding of PA with luminophores indicates the charge transfer between the PA and the luminophores (Fig. 15). The frontier molecular orbital (FMO)

Fig. 15 Frontier molecular orbitals of AC-1 and AC-1 + PA obtained from the DFT calculations using the Gaussian 09 program.

analysis further confirmed the internal charge transfer (ICT) process that occurred after the appendage of PA to the luminophores. In all the cases, the HOMO localized on the phenyl groups of the luminophore units, and the LUMO spread over on the imidazole group of the luminophores. In luminophores + PA (all luminophores), the HOMO located over the moiety of the luminophore units whereas the LUMO spread over only on the PA.

Thus, the decrease in energy after the binding of PA with luminophores clearly points out the formation of a stronger charge transfer complex of luminophores with PA.[27] The FMO orbitals of the AC-1 luminophore with PA are shown in Fig. 15. The FMO orbitals of the remaining luminophores (AC-2 to AC-6) with PA are shown in the ESI† (Fig. S54–S58).

Conclusion

In summary, we have reported six novel acenaphthene-imidazole luminophores designed and synthesized for the sensitive and selective detection of nitroaromatics in the solution and solid states. To the best of our knowledge, these luminophores are the first examples of acenaphthene-imidazole-based luminophores, which are potential candidates for the detection of trace amounts of picric acid. The detection limits of all the luminophores are in the range of 50–450 ppb. Fluorescence quenching of all the luminophores with PA has been studied with the help of emission spectra, ^{1}H NMR spectroscopy and single-crystal XRD. Using DFT analysis, the HOMO–LUMO energy levels and emission properties of all the luminophores were investigated theoretically. The chemosensing behavior of all the luminophores was confirmed by the lifetime and TD-DFT analyses. The lowest detection limit of AC-2 and AC-6 is attributed to the PET effect (i.e., the easier transfer of electrons from the AC luminophores to the PA). Compared to all the luminophores, AC-2 and AC-6 showed a higher quenching efficiency towards PA.

Experimental studies

Materials

All the reagents were used as purchased without any further purification. All the operations involving air-sensitive reagents were performed under a dry nitrogen atmosphere. The procedure for the synthesis of 4-(9H-carbazol-9-yl)benzaldehyde[18] and the luminophores[29] was adopted from the literature and modified accordingly.

General information for measurements

The ^{1}H NMR spectra were recorded using a BRUKER AV 400 Avance-III (400 MHz) instrument with tetramethylsilane as the internal standard. All the luminophores and nitroaromatics were taken in 10^{-4} M concentration. The absorption and photoluminescence (PL) excitation and the emission spectra of the synthesized luminophores were recorded using a SHIMADZU UV-2450 spectrophotometer and a HORIBAFLUOROMAX-4P spectrophotometer, respectively. The absolute fluorescence quantum yield was measured using an Edinburgh spectrofluorometer FS5 with an SC-30 integrating sphere. The photoluminescence lifetime of the dyes was measured at 298 K with an Edinburgh Instruments FLS 980 based on the time-correlated single photon counting technology upon the corresponding excitation for all the luminophores. A pulsed xenon lamp was used as the excitation source, and the signals were detected with a photomultiplier. The cyclic voltammetry experiments were performed in dimethylformamide

solution containing 0.1 M tert-butyl ammonium perchlorate using Ag/AgCl as the reference electrode at a scan rate of 100 mV s^{-1} with an AUTOLAB 302N modular potentiostat. The CIE color chromaticity coordinates of the phosphor were calculated from the emission spectral values using MATLAB software. All the chemosensing analyses were performed in THF solvent.

Computational details

The molecules under study were first optimized in the gas phase using density functional theory and the Becke three-parameter Lee–Yang–Parr (B3LYP) form for the exchange–correlation potential and the 6-31G(d,p) basis set.[30] All the structures were found to be in the minima of the potential energy surface as the normal mode of frequencies was positive. After that, the UV-Vis spectra calculations were carried out using time-dependent density functional theory (TD-DFT)[31] with gas-phase optimized geometries. It is expected that the geometry of the molecules will change in the solvent phase in comparison with that in the gas phase, and hence the optimization of the geometries in the solvent phase has also been carried out. We found that there is no prominent change in the geometries of the molecules. As the UV-Vis experiment was performed in the solution phase, we also calculated the UV-Vis spectra in the solvent phase by using the polarizable continuum model (PCM)[32] approach within the TD-DFT methodology. The singlet and triplet energy calculations were performed by using the TD-SCF and B3LYP/6-31G(P) approaches. All the calculations were carried out using the Gaussian09 W[33] and Gaussian View suite of programs. The optoelectronic properties including FMOs, and the absorption and emission spectra were calculated using TD-DFT analysis.

Synthesis

Synthesis of 4-(9H-carbazol-9-yl)benzaldehyde. 9H-Carbazole (4.0 g, 23.92 mmol), 4-bromobenzaldehyde (5.2 g, 28.11 mmol), K_2CO_3 (13.20 g, 95.69 mmol), copper powder (3.04 g, 47.84 mmol) and dibenzo-18-crown-6 (0.63 g, 2.39 mmol) were dissolved in anhydrous DMF (50 mL) under a nitrogen atmosphere and refluxed for 48 h. Then, the mixture was cooled down to room temperature and filtered. The filtrate was poured into distilled water (300 mL) and stirred for 30 min. The crude product was collected by filtration and was purified by column chromatography (silica gel) eluting with a mixture of ethyl acetate : n-hexane (2 : 1; v/v) to give a light-yellow solid (4.5 g, 69%): ^{1}HNMR (400 MHz) – δ 10.12 (s, 1H), 8.17–8.13 (m, 4H), 7.78 (d, 2H), 7.54–7.30 (m, 6H).

General procedure for the synthesis of luminophores. Acenapthequinone (5.5 mmol), 4-(9H-carbazol-9-yl)benzaldehyde (3.6 mmol), and an equivalent amount of aniline derivative $C_6H_5NH_2R$ (R = H, m-CF$_3$, p-CF$_3$, m-CN, p-CH$_3$, diethylfluorene), together with ammonium acetate (36 mmol), were dissolved in glacial acetic acid (15 mL) under a nitrogen atmosphere and refluxed for about 24 h. The mixture was then poured into water and extracted with DCM. The extracted product was made into a crude product by adding silica gel. This crude was purified by column chromatography (silica gel) eluting with a mixture of ethylacetate : petroleum ether (3 : 7 v/v) to give a yellow or

yellow-orange solid. The detailed NMR data are mentioned in the ESI.†

Conflicts of interest

There are no conflicts to declare.

Acknowledgements

References

1 Y. Salinas, R. Martínez-Máñez, M. D. Marcos, F. Sancenón, A. M. Costero, M. Parra and S. Gil, *Chem. Soc. Rev.*, 2012, **41**, 1261–1296.

2 (a) V. Pimienta, R. Etchenique and T. Buhse, *J. Phys. Chem. A*, 2001, **105**, 10037; (b) J. Shen, J. Zhang, Y. Zuo, L. Wang, X. Sun, J. Li, W. Han and R. He, *J. Hazard. Mater.*, 2009, **163**, 1199; (c) G. Anderson, J. D. Lamar and P. T. Charles, *Environ. Sci. Technol.*, 2007, **41**, 2888–12893; (d) J. F. Wyman, M. P. Serve, D. W. Hobson, L. H. Lee and D. E. J. Uddin, *J. Toxicol. Environ. Health, Part A*, 1992, **37**, 313–327.

3 (a) J. Yinon, *Anal. Chem.*, 2003, **75**, 99A; (b) A. M. Rouhi, *Chem. Eng. News*, 1997, **75**, 14; (c) J. I. Steinfeld and J. Wormhoudt, *Annu. Rev. Phys. Chem.*, 1998, **49**, 203.

4 (a) H. Du, G. He, T. Liu, L. Ding and Y. Fang, *J. Photochem. Photobiol., A*, 2011, **217**, 356; (b) D. Ownby, J. Belden, G. Lotufo and M. Lydy, *Chemosphere*, 2005, **58**, 1153; (c) D. Ownby, J. Belden, G. Lotufo and M. Lydy, *Chemosphere*, 2005, **58**, 1161; (d) E. Etnier, *Regul. Toxicol. Pharmacol.*, 1989, **9**, 147; (e) M. Honeycutt, A. Jarvis and V. McFairland, *Ecotoxicol. Environ. Saf.*, 1996, **35**, 282; (f) P. Robidoux, J. Hawari and S. Thiboutot, *Environ. Toxicol. Chem.*, 1999, **23**, 1026.

5 (a) M. E. Germain and M. J. Knapp, *Chem. Soc. Rev.*, 2009, **38**, 2543–2555; (b) R. G. Ewing, D. A. Atkinson, G. A. Eiceman and G. J. Ewing, *Talanta*, 2001, **54**, 515–529; (c) S. Singh, V. K. Meena, B. Mizaikoff, S. P. Singh and C. R. Surid, *Anal. Methods*, 2013, **8**, 7158–7169.

6 K. P. Carter, A. M. Young and A. E. Palmer, *Chem. Rev.*, 2014, **114**, 4564–4601.

7 (a) B. Valeur, *Molecular Fluorescence*, Wiley-VCH, Weinheim, Germany, 2001; (b) D. J. Irvine, M. A. Purbhoo, M. Krogsgaard and M. M. Davis, *Nature*, 2002, **419**, 845; (c) T. W. Bell and N. M. Hext, *Chem. Soc. Rev.*, 2004, **33**, 589.

8 H. Lu, L. Q. Xiong, H. Z. Liu, M. X. Yu, Z. Shen, F. Y. Li and X. Z. You, *Org. Biomol. Chem.*, 2009, **7**, 2554.

9 (a) E. M. Nolan and S. J. Lippard, *Chem. Rev.*, 2008, **108**, 3443; (b) B. Tang, B. Y. Ding, K. H. Xu and L. L. Tong, *Chem. – Eur. J.*, 2009, **15**, 3147; (c) A. Thibon and V. C. Pierre, *J. Am. Chem. Soc.*, 2009, **131**, 434.

10 (a) M. X. Yu, M. Shi, Z. G. Chen, F. Y. Li, X. X. Li, Y. H. Gao, J. Xu, H. Yang, Z. G. Zhou, T. Yi and C. H. Huang, *Chem. – Eur. J.*, 2008, **14**, 6892; (b) Z. G. Zhou, M. X. Yu, H. Yang, K. W. Huang, F. Y. Li, T. Yi and C. H. Huang, *Chem. Commun.*, 2008, 3387; (c) K. W. Huang, H. Yang, Z. G. Zhou, M. X. Yu, F. Y. Li, X. Gao, T. Yi and C. H. Huang, *Org. Lett.*, 2008, **10**, 2557; (d) M. X. Yu, F. Y. Li, Z. G. Chen, H. Hu, C. Zhan, C. Yang and C. H. Huang, *Anal. Chem.*, 2009, **81**, 930; (e) M. Taki, M. Desaki, A. Ojida, S. Iyoshi, T. Hirayama, I. Hamachi and Y. Yamamoto, *J. Am. Chem. Soc.*, 2008, **130**, 12564.

11 (a) Z. Hu, B. J. Deibert and J. Li, *Chem. Soc. Rev.*, 2014, **43**, 5815–5840; (b) X. C. Sun, Y. Wang and Y. Lei, *Chem. Soc. Rev.*, 2015, **44**, 8019–8061; (c) K. S. Bejoymohandas, T. M. George, S. Bhattacharya, S. Natarajanb and M. L. P. Reddy, *J. Mater. Chem. C*, 2014, **2**, 515–523.

12 (a) K. Shen, Z. M. Ju, L. Qin, T. Wang and H. G. Zheng, *Dyes Pigm.*, 2017, **136**, 515–521; (b) K. K. Kartha, S. S. Babu, S. Srinivasan and A. Ajayaghosh, *J. Am. Chem. Soc.*, 2012, **134**, 4834; (c) M. Kumar, V. Vij and V. Bhalla, *Langmuir*, 2012, **28**(33), 12417–12421.

13 (a) J. Tagare and S. Vaidyanathan, *J. Mater. Chem. C*, 2018, **6**(38), 10138–10173; (b) A. B. Kajjam, D. K. Dubey, R. A. K. Yadav, J.-H. Jou and V. Sivakumar, *Mater. Today Chem.*, 2019, **14**, 100201; (c) J. Tagare, H. Ulla, M. N. Satyanarayan and S. Vaidyanathan, *J. Lumin.*, 2018, **194**, 600–609; (d) J. Tagare, D. K. Dubey, J. H. Jou and S. Vaidyanathan, *Dyes Pigm.*, 2018, **160**, 944–956; (e) R. Devi, K. Singh and S. Vaidyanathan, *J. Mater. Chem. C*, 2020, **8**(25), 8643–8653; (f) R. Devi, R. Boddula, J. Tagare, A. B. Kajjam, K. Singh and S. Vaidyanathan, *J. Mater. Chem. C*, 2020, **8**(34), 11715–11726; (g) R. Devi, M. Rajendran, K. Singh, R. Pal and S. Vaidyanathan, *J. Mater. Chem. C*, 2021, **9**, 6618–6633.

14 (a) Z. Z. Mao, Z. Y. Wang, J. N. Li, X. M. Song and Y. F. Luo, *Synth. Commun.*, 2010, **40**, 1963–1977; (b) R. Frei, A. S. Breitbach and H. E. Blackwell, *Angew. Chem., Int. Ed.*, 2012, **51**, 5226–5229; (c) B. Narasimhan, D. Sharma and P. Kumar, *Med. Chem. Res.*, 2012, **21**, 269–283; (d) P. Peng, J. F. Xiong, G. Z. Mo, J. L. Zheng, R. H. Chen, X. Y. Chen and Z. Y. Wang, *Amino Acids*, 2014, **46**, 2427–2433.

15 K. Zhu, V. N. Vukotic and S. J. Loeb, *Angew. Chem., Int. Ed.*, 2012, **51**, 2168–2172.

16 Q. T. He, X. P. Li, Y. Liu, Z. Q. Yu, W. Wang and C. Y. Su, *Angew. Chem., Int. Ed.*, 2009, **48**, 6156–6159.

17 Z. Guo, N. R. Song, J. H. Moon, M. Kim, E. J. Jun, J. Choi, J. Y. Lee, C. W. Bielawski, J. L. Sessler and J. J. Yoon, *J. Am. Chem. Soc.*, 2012, **134**, 17846–17849.

18 (a) J.-F. Xiong, J.-X. Li, G.-Z. Mo, J.-P. Huo, J.-Y. Liu, X.-Y. Chen and Z.-Y. Wang, *J. Org. Chem.*, 2014, **79**, 11619–11630; (b) B. Roy, A. K. Bar, B. Gole and P. S. Mukherjee, *J. Org. Chem.*, 2013, **78**, 1306–1310.

19 (a) J. Li, B. Zhanga, W. Yang, S. Jia, M. Xue, W. Guangcheng, F. Sihong, C. Lina and Y. Li, *Nat. Prod. Res.*, 2019, **35**,

1307–1312; (b) U. El-Ayaan, A. A.-M. Abdel-Aziz and S. Al-Shihry, *Eur. J. Med. Chem.*, 2007, **42**, 1325–1333; (c) W. Zhu, M. Dai, Y. Xu and X. Qian, *Bioorg. Med. Chem.*, 2008, **16**, 3255–3260; (d) J. E. Mc Davids and T. C. Daniels, *J. Am. Pharm. Assoc.*, 1951, **40**, 325–326; (e) U. El-Ayaan and A. A.-M. Abdel-Aziz, *Eur. J. Med. Chem.*, 2005, **40**, 1214–1221; (f) S. D. Levine; N. Brunswick; I. T. Harper and K. Park, Acenaphthene carboxamides, *US Pat.*, 3732299A, 1973; (g) M. Eagleson, *Concise Encyclopedia Chemistry*, Walter de Gruyter, Berlin, Germany, 1993, p. 3.

20 (a) J. Carole, M.-A. Monique, J. Andrieux, S. Kloubert, J. A. Boutin, J.-P. Nicolas, C. Bennejean, P. Delagrange and M. Langlois, *J. Med. Chem.*, 2000, **43**, 4051–4062; (b) Y.-M. Xie, Y. Deng, X.-Y. Dai, J. Liu, L. Ouyang, Y.-Q. Wei and Y.-L. Zhao, *Molecules*, 2011, **16**, 2519–2526; (c) W. R. N. Williamson, Pharmacologically active acenaphthene derivatives, *US Pat.*, US4246281A, 1979.

21 D. C. Santra, M. K. Bera, P. K. Sukul and S. Malik, Charge-transfer-induced fluorescence quenching of anthracene derivatives and selective detection of picric acid, *Chem. – Eur. J.*, 2016, **22**, 2012–2019.

22 D. Harvey, *Modern Analytical Chemistry*, Boston, 2000, p. 798.

23 (a) S. Sandhu, R. Kumar, P. Singh, A. Mahajan, M. Kaur and S. Kumar, *ACS Appl. Mater. Interfaces*, 2015, **7**, 10491–10500; (b) V. Bhalla, A. Gupta and M. Kumar, *Org. Lett.*, 2012, **14**, 3112–3115; (c) P. Mazumdar, S. Maity, M. Shyamal, D. Das, G. P. Sahoo and A. Misra, *Phys. Chem. Chem. Phys.*, 2016, **18**, 7055–7067; (d) M. Shyamal, S. Maity, P. Mazumdar, G. P. Sahoo, R. Maity and A. Misra, *J. Photochem. Photobiol., A*, 2017, **342**, 1–14.

24 (a) S. Pramanik, V. Bhalla and M. Kumar, *Anal. Chim. Acta*, 2013, **793**, 99–106; (b) S. Shanmugaraju, H. Jadhav, Y. P. Patil and P. S. Mukherjee, *Inorg. Chem.*, 2012, **51**,

13072–13074; (c) J. Wang, J. Mei, W. Yuan, P. Lu, A. Qin, J. Sun, Y. Ma and B. Z. Tang, *J. Mater. Chem.*, 2011, **21**, 4056–4059; (d) D. Li, J. Liu, R. T. K. Kwok, Z. Liang, B. Z. Tang and J. Yu, *Chem. Commun.*, 2012, **48**, 7167–7169.

25 (a) N. Venkatramaiah, S. Kumar and S. Patil, *Chem. – Eur. J.*, 2012, **18**, 14745–14751; (b) A. B. Kajjam, D. K. Dubey, R. A. K. Yadav, J.-H. Jou and V. Sivakumar, *Mater. Today Chem.*, 2019, **14**, 100201; (c) S.-H. Chen, K. Jiang, J.-Y. Lin, K. Yang, X.-Y. Cao, X.-Y. Luo and Z.-Y. Wang, *J. Mater. Chem. C*, 2020, **8**, 8257–8267.

26 K. J. Albert, N. S. Lewis, C. L. Schauer, G. A. Sotzing, S. E. Stitzel, T. P. Vaid and D. R. Walt, Cross-reactive chemical sensor arrays, *Chem. Rev.*, 2000, **100**, 2595–2626.

27 (a) P. Jana, S. Maity, S. K. Maity, P. K. Ghorai and D. Haldar, *Soft Matter*, 2012, **8**, 5621; (b) G. Sivaraman, V. Balasubramanian and D. Chellappa, *RSC Adv.*, 2014, **4**, 30828.

28 Z. C. Liang, H. Chen, X. H. Wang and R. C. Sun, *Dyes Pigm.*, 2016, **125**, 367–374.

29 C. J. Kuo, T. Y. Li, C. C. Lien, C. H. Liu, F. I. Wu and M. J. Huang, *J. Mater. Chem.*, 2009, **19**, 1865–1871.

30 (a) A. Becke, *J. Chem. Phys.*, 1993, **98**, 5648; (b) C. Lee, W. Yang and R. G. Parr, *Phys. Rev. B: Condens. Matter Mater. Phys.*, 1988, **37**, 785–5789.

31 (a) R. Bauernschmitt and R. Ahlrichs, *Chem. Phys. Lett.*, 1996, **256**, 454–464; (b) G. Scalmani, M. J. Frisch, B. Mennucci, J. Tomasi, R. Cammi and V. Barone, *J. Chem. Phys.*, 2006, **124**, 094107.

32 (a) J. Tomasi, B. Mennucci and R. Cammi, *Chem. Rev.*, 2005, **105**, 2999–3093; (b) A. B. Kajjam, P. S. V. Kumar, V. Subramanian and V. Sivakumar, *Phys. Chem. Chem. Phys.*, 2018, **20**, 4490–4501.

33 M. J. Frisch, *et al.*, *Gaussian 09, Revision D.01*, Gaussian, Inc., Wallingford, CT, 2009.